PHYSICAL REVIEW A **85**, 031805(R) (2012)

Strongly enhanced light-matter interaction in a hybrid photonic-plasmonic resonator

Yun-Feng Xiao,* Yong-Chun Liu,† Bei-Bei Li, You-Ling Chen, Yan Li, and Qihuang Gong‡
State Key Lab for Mesoscopic Physics, Department of Physics, Peking University, People's Republic of China
(Received 7 July 2011; revised manuscript received 24 September 2011; published 27 March 2012)

We propose a hybrid photonic-plasmonic resonant structure which consists of a metal nanoparticle (MNP) and a whispering-gallery-mode (WGM) microcavity. It is found that the hybrid mode enables a strong interaction between the light and matter, and the single-atom cooperativity is enhanced by more than two orders of magnitude compared to that in a bare WGM microcavity. This improvement originates from two aspects: the MNP offers a highly enhanced local field in the vicinity of an emitter, and, interestingly, the high-Q property of WGMs can be maintained in the presence of the MNP. Thus the present system has advantages over a single microcavity or a single MNP, and holds potential in quantum optics, nonlinear optics, and highly sensitive biosensing.

DOI: 10.1103/PhysRevA.85.031805 PACS number(s): 42.50.Pq, 42.50.Ct, 42.50.Dv, 78.67.−n

Owing to the size mismatch between light and single emitters such as single atoms, the interaction between them is very weak, so that it is of importance to create a light-matter interface enabling strong interactions. One way to bridge this mismatch is to employ the strong interaction within cavity quantum electrodynamics (QED) [1,2]. Cavity QED offers an almost ideal platform for the study of physics at the interface of classical and quantum mechanics, and provides a technology for various devices in the field of quantum information [3–5]. Experiments on the strong-coupling regime in cavity QED have made great advances over the past two decades [6]. Among them, whispering-gallery-mode (WGM) microcavities [7] are promising because they possess an ultrahigh-quality (Q) factor and allow for mass production on a chip. However, the relatively large cavity mode volume makes it difficult to realize strong coupling. On the other hand, due to localized surface plasmon resonance (LSPR) [8], metal nanoparticles (MNPs) [9] enable subwavelength confinement of the optical field [10–14]. Unfortunately, MNPs suffer from serious absorption and scattering losses.

Against this backdrop, in this Rapid Communication, taking advantages from both ultralow-loss WGMs and highly localized plasmons, we propose a WGM microcavity-MNP resonant system. In this composite system, the high-Q WGM microcavity serves as a low-loss storage of the optical field, while the MNP plays the role of an optical antenna which creates a hot spot and magnifies the local optical field. Interestingly, the high-Q property of WGMs can be maintained in the presence of the MNP. As a result, the cooperativity parameter (defined as $C = 2G^2/\kappa\gamma_s$ [15], with G being the single-photon coupling strength, γ_s the spontaneous decay of the emitter, and κ the decay of the cavity field) achieves a more than 100-fold increase compared with that of the WGM cavity alone. It should be pointed out that this composite cavity QED structure is significantly different from previous designs, where a silica disk or toroid was completely covered with a metal layer, which led to strong degrading of the Q factor [16,17].

Figure 1 illustrates a schematic of the system. A MNP is located on the surface of a microtoroidal cavity [18] which supports twin counterpropagating WGMs with degenerate frequency ω_c (neglecting the coupling between these two modes arising from surface-roughness-induced scattering). A dipole emitter (ground state $|g\rangle$, excited state $|e\rangle$, energy spacing $\hbar\omega_e$, and dipole moment $\mu\hat{\mathbf{e}}_x$) is placed in the vicinity of the MNP. Experimentally we can use atomic force microscope (AFM) manipulation to controllably position the MNP and the dipole emitter [19,20]. Alternatively, we can also use gold-coated fiber taper tip to play the role of the MNP, in analogy to the method utilizing the fiber tip to simulate a dielectric nanosphere [21]. A tapered fiber is used to couple light into and out of the microcavity. We consider TE-polarized WGMs, with the dominant electric field component in the $\hat{\mathbf{e}}_x$ direction. In the absence of the MNP, the Jaynes-Cummings Hamiltonian reads $H_c = \omega_c\sum_n a_n^\dagger a_n + \frac{1}{2}\omega_e\sigma_z + G_c\sum_n(a_n^\dagger\sigma_- + a_n\sigma_+)$, where $\sigma_-=\sigma_+^\dagger=|g\rangle\langle e|$, $\sigma_z=|e\rangle\langle e| - |g\rangle\langle g|$, a_n ($a_n^\dagger$) denotes the annihilation (creation) operator of the WGMs with $n =$ CW (CCW) corresponding to the clockwise (counterclockwise) propagating mode. The single-photon coupling strength (vacuum Rabi frequency) is given by $G_c = \mu f_c(\mathbf{R})[\omega_c/(2\hbar\varepsilon_0\varepsilon_c V_c)]^{1/2}$, where ε_0 is the permittivity of vacuum, ε_c is the relative permittivity of the microcavity, and V_c and $f_c(\mathbf{R})$ denote the mode volume and normalized field distribution of the WGMs, respectively.

Now we focus on the case when a spherical MNP is placed in the vicinity of the microcavity and the dipole emitter, with the position $\mathbf{R} = \mathbf{R}_0$. The radius of the MNP r_m is much smaller than the light wavelength, so that the interaction arising from the MNP is governed by electrostatics rather than electrodynamics [22], which is confirmed by our numerical simulations [Figs. 1(c)–1(f)]. By solving Laplace's equation, we obtain the positive frequency component of the total field inside and outside the MNP: $\mathbf{E}_{c,m}^{(+)}(r,\theta) = (1-\beta)E_c^{(+)}(\mathbf{R}_0)\hat{\mathbf{e}}_x$ $(r \leqslant r_m)$, $\mathbf{E}_{c,m}^{(+)}(r,\theta) = E_c^{(+)}(\mathbf{R}_0)\hat{\mathbf{e}}_x + \beta(r_m^3/r^3)E_c^{(+)}(\mathbf{R}_0)(2\hat{\mathbf{e}}_r\cos\theta + \hat{\mathbf{e}}_\theta\sin\theta)$ $(r > r_m)$. Here the dipole emitter-induced field has been omitted in the weak excitation limit; $r = |\mathbf{R} - \mathbf{R}_0|$ and θ form a polar coordinates system; the complex coefficient β is given by $\beta = (\varepsilon_m - \varepsilon_b)/(\varepsilon_m + 2\varepsilon_b)$, where ε_m (ε_b) denotes the relative permittivity of the MNP (the surrounding medium). We can use the Drude dispersion relation $\varepsilon_m(\omega) = 1 - \omega_p^2/[\omega(\omega + i\gamma_m)]$,

*www.phy.pku.edu.cn/∼yfxiao/index.html
†ycliu@pku.edu.cn
‡qhgong@pku.edu.cn

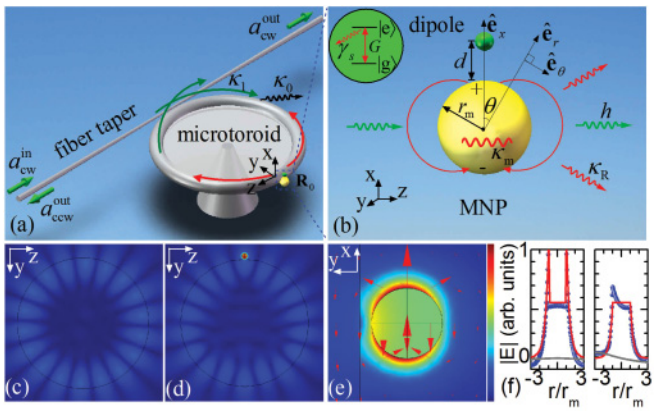

FIG. 1. (Color online) (a) Sketch of the MNP-WGM composite system (not to scale). (b) Zoomed-in view of the MNP and the dipole emitter. The inset is the energy diagram of the dipole. (c)–(e) Three-dimensional finite-element simulations of the electric field distribution. Top view of the electric field profile (c) without and (d) with the MNP. (e) Zoomed-in view of the field distribution near the MNP (azimuthal cross section). The arrows show the electric field directions. The vertical line on the left of the MNP is the cavity boundary. The colors in (c)–(e) represent the norm of the electric field ($|E|$). (f) Comparison of the electric field with (blue/dark gray dot) and without (light gray dot) MNP for $\theta = 0$ (left) and $\theta = \pi/2$ (right). The red solid curves are the theoretical result (see text). To save simulation resources, here we use a relatively small microcavity (major radius 0.8 μm) and a relatively large MNP ($r_m = 30$ nm).

where ω_p is the bulk plasma frequency and γ_m is the damping rate which accounts for energy dissipation due to ohmic losses. The LSPR [8] occurs with the dipolar plasmonic resonance frequency ω_{sp} satisfying $\mathrm{Re}[\varepsilon_m(\omega_{sp})] = -2\varepsilon_b$. In this case, $|\beta| \gg 1$, and the local field in the vicinity of the MNP is enhanced significantly.

The response of the MNP results in the redistribution of the cavity mode field, forming a hybrid photonic-plasmonic mode. The modified maximum field strength reads $|E_{c,m,\max}| = f_c(\mathbf{R}_0)|(1+2\beta)E_{c,\max}|$, and thereby the mode volume decreases to be $V_{c,m} = \varepsilon_c V_c/[\varepsilon_b|1+2\beta|^2 f_c^2(\mathbf{R}_0)]$, which approximately scales as $|\beta|^2$ times smaller than the bare cavity case. Thus the MNP effectively plays the role of an optical antenna which (i) confines the photon energy, (ii) reduces the mode volume, and (iii) magnifies the local field. For the longitudinal case ($\theta = 0$), the modified single-photon coupling strength $G_{c,m}$ is calculated to be $|1+2\beta r_m^3/r^3|$ times as large as G_c.

In this composite cavity QED system, a key question is whether the MNP significantly degrades the high-Q property of WGMs. The MNP-induced decay includes two contributions: scattering and absorption losses. For the subwavelength MNP, the scattering interaction can be modeled in a dipole approximation, where the electric field of the input wave induces a dipole moment in it [21]. On one hand, this scattering interaction mixes the two counterpropagating modes, described by the Hamiltonian $H_1 = -\frac{1}{2}\mathbf{p}_m \cdot \mathbf{E}_{c,m}(\mathbf{R}_0)$, where $\mathbf{p}_m = \varepsilon_0\varepsilon_b\alpha E_c^{(+)}(\mathbf{R}_0)\hat{\mathbf{e}}_x + \mathrm{H.c.}$ is the polarization and $\alpha = 4\pi r_m^3\beta$ is the polarizability of the spherical MNP. It can be simplified as $H_1 = h\sum_{n,n'} a_n^\dagger a_{n'}$, where $n,n' = \mathrm{CW},\mathrm{CCW}$, and $h = 2\pi r_m^3\varepsilon_b\omega_c|\beta|^2 f_c^2(\mathbf{R}_0)/(\varepsilon_c V_c)$ is the coupling strength. On the other hand, the scattering results in the decay from WGMs to reservoir modes, described by the Hamiltonian $H_2 = -\frac{1}{2}\sum_j[\mathbf{p}_m \cdot \mathbf{E}_j(\mathbf{R}_0) + \mathbf{p}_j \cdot \mathbf{E}_{c,m}(\mathbf{R}_0)]$, where $\mathbf{E}_j(\mathbf{R}_0)$ is the electric field for the jth reservoir mode and $\mathbf{p}_j$ is reservoir-induced polarization of the MNP. Taking the Weisskopf-Wigner semi-QED treatment [21], the scattering process results in a radiation energy decay of the WGMs, which takes an analogous form of spontaneous emission. After tracing out the freedom of the reservoir modes, we obtain the effective Hamiltonian $H_{2,\mathrm{eff}} = -i\kappa_R\sum_{n,n'} a_n^\dagger a_{n'}$ with the damping rate $\kappa_R = \varepsilon_b^{5/2}(4\pi r_m^3)^2|\beta|^4\omega_c^4 f_c^2(\mathbf{R}_0)/(6\pi c^3\varepsilon_c V_c)$, where c is the speed of light in vacuum.

The absorption of the MNP results in ohmic losses, characterized by the imaginary part of the metal's permittivity. Thus this energy dissipation can be described by the non-Hermitian Hamiltonian $H_{3,\mathrm{eff}} = \frac{i}{2}\varepsilon_0\int_{|\mathbf{R}-\mathbf{R}_0|\le r_m}\mathrm{Im}[d(\omega\varepsilon_m(\omega))/d\omega]|_{\omega=\omega_c}E_{c,m}(\mathbf{R})^2 d\mathbf{R}^3$, rewritten as $H_{3,\mathrm{eff}} = -i\kappa_m\sum_{n,n'} a_n^\dagger a_{n'}$, with the decay rate $\kappa_m = 4\pi r_m^3|1-\beta|^2\omega_p^2\gamma_m f_c^2(\mathbf{R}_0)/(3\varepsilon_c\omega_c^2 V_c)$. In current case, the energy fraction of the hybrid mode within the MNP is very small (<0.01%), resulting in a minor κ_m.

Now we arrive at the overall Hamiltonian of the composite system $H_{c,m} = H_c + H_1 + H_{2,\mathrm{eff}} + H_{3,\mathrm{eff}}$. Next we consider specific examples. Different from a low-Q photonic crystal nanocavity [23], here we focus on the enhanced light-matter interaction in a silica microtoroidal cavity [18] which possesses a relatively high intrinsic quality factor $Q_0 = 10^7$. We use a typical toroidal microcavity with the major and minor radii being 30 and 3 μm, respectively. For such a cavity in air, $\varepsilon_c = 1.45^2$, $\varepsilon_b = 1$, we obtain $V_c \sim 200\ \mu\mathrm{m}^3$ [corresponding to $4000(\lambda/n)^3$] and $f_c(\mathbf{R}_0) \sim 0.3$ using finite-element simulations. We set the cavity-taper coupling strength $\kappa_1 = 5\kappa_0$, where $\kappa_0 = \omega_c/Q_0$ denotes the intrinsic damping of the WGMs. Here we use large κ_1 so as to realize near critical coupling in the presence of the MNP, which brings about additional decays. For a gold MNP, the permittivity can be extracted from the experimental data [24], with $\omega_p \sim 6\times 10^{15}$ Hz (corresponding to the LSPR wavelength of 540 nm) and $\gamma_m \sim 3\times 10^{14}$ Hz. For the dipole emitter, we can use a chemically synthesized cadmium selenide (CdSe) quantum dot, with a dipole moment $\mu = 2.4\times 10^{-28}$ C·m [13], a spontaneous emission rate $\gamma_s = \varepsilon_b^{1/2}\mu^2\omega_e^3/(3\pi\epsilon_0\hbar c^3) = 2\pi\times 1.6$ GHz, and a emitter-cavity detuning $\Delta_{ec} \equiv \omega_e - \omega_c = 0$. To focus on the physics, the size of the quantum dot is assumed to be small so that its mesoscopic effects [25] can be neglected. Note that for a more general emitter such as an atom or a dye molecule, the size can be considered to be zero. In Fig. 2(a) we plot the cooperativity enhancement as a function of r_m and d (the distance between the dipole emitter and the surface of the MNP). It is shown that the enhancement can exceed more than two orders of magnitude, and there is enough parameter space for large enhancement. As an example, we set $d = 3$ nm, corresponding to the horizontal line in Fig. 2(a). At this distance, the charge carrier tunneling can be safely avoided [26,27]. With a MNP of specific geometry [28], the dipole's emission to dark multipolar plasmonic resonances, which can be regarded as an addition spontaneous decay of the dipole emitter and is largely related to the concept of the "quenching"

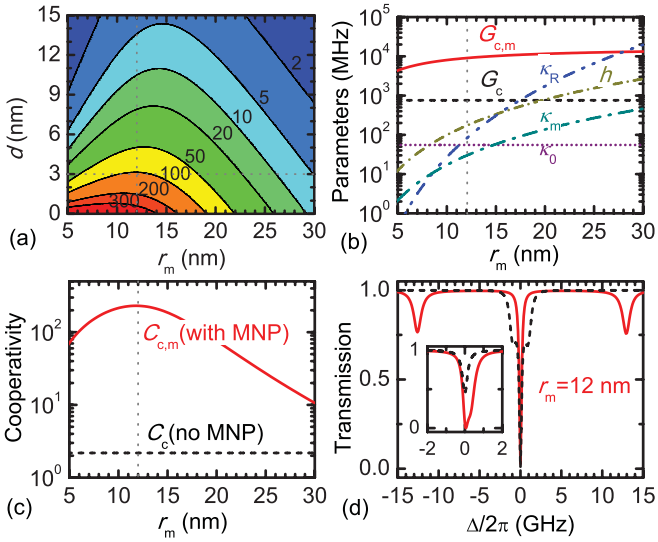

FIG. 2. (Color online) (a) Contour plot of the cooperativity enhancement ($C_{c,m}/C_c$) vs r_m and d. (b) Parameters $\{G_c, G_{c,m}, h, \kappa_0, \kappa_R, \kappa_m\}/2\pi$ vs r_m. (c) Cooperativity with the presence of the MNP ($C_{c,m}$) and with its absence (C_c). The horizontal line in (a) corresponds to $d = 3$ nm. The vertical lines in (a)–(c) correspond to $r_m = 12$ nm. (d) Transmission spectra for $r_m = 12$ nm and $d = 3$ nm in the presence of the dipole, with (solid line) and without the MNP (dashed line). $\{G_c, G_{c,m}, h, \kappa_0, \kappa_R, \kappa_m\}/2\pi = \{760, 9000, 170, 55, 80, 30\}$ MHz. The input-cavity detuning $\Delta = \omega - \omega_c$. The inset is for no dipole case. For (b)–(d), $d = 3$ nm; For (a)–(d), the cavity-MNP detuning $\Delta_{sp} = 0$.

in the fluorescence measurement, will be significantly reduced to a minor efficiency of 1–3%. The metal absorption in the hybrid mode, also related to "quenching," is extremely weak due to the ultrasmall energy fraction (<0.01%) within the MNP, which differs from the pure plasmonic resonant system. When LSPR occurs ($\omega_c = \omega_{sp}$), we obtain $|\beta| = 11.5$. Figure 2(b) plots the characteristic parameters depending on the radius of the MNP. It explicitly shows that the dipole-field single-photon coupling strength with the help of the MNP ($G_{c,m}$, solid line) can be more than ten times larger than that without the MNP (G_c, dashed line), with achievable $G_{c,m}/2\pi \simeq 13$ GHz. When r_m is small, the extra decays (κ_R, κ_m) are smaller than the intrinsic cavity decay κ_0. Therefore, for a small MNP, the enhancement of the local field can be quite strong, while the high-Q property of the system is surprisingly maintained. In Fig. 2(c), we plot the cooperativity parameter as a function of r_m both in the presence of the MNP and in its absence. We can see that for $r_m \simeq 12$ nm, the cooperativity is enhanced more than 100-fold, with the corresponding $G_{c,m}/2\pi = 9$ GHz.

To probe the enhanced light-matter interaction, we use weak monochromatic clockwise propagating light input a_{cw}^{in}. By utilizing the Heisenberg-Langevin equations and the input-output theory [29,30], we obtain the cavity transmission spectra for $r_m = 12$ nm in Fig. 2(d). When the MNP is absent, the vacuum Rabi splitting cannot be resolved. On the contrary, with the help of the MNP, a mode splitting of $2\sqrt{2}G_{c,m}$ can be observed. This splitting is completely the cavity QED effect and the scattering of the MNP has

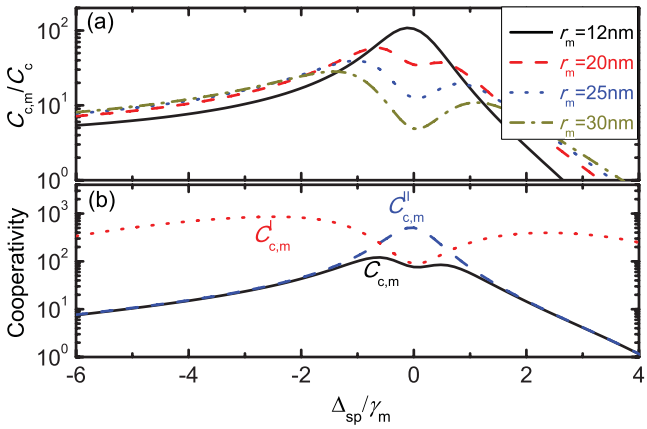

FIG. 3. (Color online) (a) Cooperativity enhancement ($C_{c,m}/C_c$) vs cavity-MNP detuning Δ_{sp}/γ_m for several typical r_m. (b) The cooperativity parameters $C_{c,m}$, $C^I_{c,m}$ (near resonance, $|\Delta_{sp}| \ll \gamma_m$), and $C^{II}_{c,m}$ (off resonance, $|\Delta_{sp}| \gg \gamma_m$) for $r_m = 20$ nm.

no contribution to it. To demonstrate this, in the inset of Fig. 2(d), we plot the transmission spectra for the no dipole emitter case. As expected, no splitting is observed, where the asymmetry spectrum in the presence of the MNP is due to the scattering-induced mixing of the WGMs.

One distinct property of LSPR is that the plasmon excitation covers a broad bandwidth. In fact, the optimal condition for the improvement of strong coupling does not occur at the exact cavity-MNP resonance for large-size MNP, where the MNP-induced decay exceeds the original decay. This is verified in Fig. 3(a), which displays the cooperativity parameters for cavity-MNP detuning ($\Delta_{sp} \equiv \omega_c - \omega_{sp}$) varying from $-6\gamma_m$ to $4\gamma_m$. It is interesting that $C_{c,m}/C_c$ arrives at a local minimum at $\Delta_{sp} = 0$ for a large r_m. The underlying physics is that the MNP-induced decay contributes more than the field enhancement. To explain this more clearly, we plot the cooperativity for $r_m = 20$ nm in Fig. 3(b). In the near-resonance region, the loss induced by the MNP is dominant, and thereby $C_{c,m} \simeq C^I_{c,m} = 2G^2_{c,m}/[\gamma_s(\kappa_R + \kappa_m)]$, while in the off-resonance region, these decays decrease to a low level, yielding $C_{c,m} \simeq C^{II}_{c,m} = 2G^2_{c,m}/[\gamma_s(\kappa_0 + \kappa_1)]$. It is shown that, for the red cavity-MNP detuning case, the cooperativity can maintain a high value over a broad range. Note that $\Delta_{sp} = 0, -6\gamma_m$ corresponds to wavelengths of 540 and 1130 nm, respectively. Moreover, even for $r_m = 30$ nm, the cooperativity can still be enhanced by 30-fold for a suitable detuning.

Enhancing the strong coupling in cavity QED is of crucial importance in high-speed operation of the quantum gate and fast generation of the entangled state, as illustrated in Fig. 4(a). These can be obtained among two or more identical MNP-atom molecules localized near the microcavity. The atoms interact with a shared cavity mode and a classical laser field is applied to control the evolution among them. Typically, to suppress the atomic spontaneous emission, the system usually works in the large atom-field detuning limit ($\Delta_{ec} \gg G$) [3,31]. For a conventional cavity QED setup without MNPs, this large detuning limit is theoretically feasible, but may not be applicable because the effective interacting strength ($\propto G^2/\Delta_{ec}$) decreases significantly and the Rabi oscillation

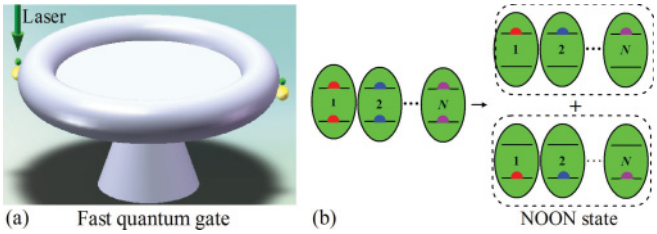

FIG. 4. (Color online) Illustration of the fast quantum gate operation (a) and NOON state generation (b).

becomes slow. On the contrary, with the help of MNPs, the effective interaction is significantly enhanced. As an example, the effective interacting strength can be improved 100-fold with the help of MNPs. This means that the quantum gate operation and the entanglement generation can finish in a much shorter time, and the system allows for many more operations within the coherence time.

Other examples include the fast generation of the spin squeezed state [32] and the N dipole emitters maximally entangled state (also known as the NOON state) [33]. To this end, N identical MNP-atom molecules are positioned around the cavity. In the large detuning case, the effective Hamiltonian is given by $H_{\rm eff} = \chi(J_z - J_z^2)$, where $\chi = 2G_{\rm c,m}^2/(\Delta_{\rm ec} - Nh)$ and $J_z = \frac{1}{2}\sum_{j=1}^{N}\sigma_z^{(j)}$. This Hamiltonian is the generalized one-axis-twisting type [34], which implies that it is capable of performing spin squeezing. To create the NOON state, dipole emitters are initially prepared in the superposition state $2^{-N/2}(|g\rangle + |e\rangle)^{\otimes N}$ using a fast $\pi/2$ pulse. Next the system undergoes free evolution for $\chi t = \pi/2$. Then a second $\pi/2$ pulse is applied to finally create the NOON state $(|g\rangle^{\otimes N} + |e\rangle^{\otimes N})/\sqrt{2}$, as described in Fig. 4(b). Previously this scheme is subjected to the weak nonlinearity and experimentally it is a challenge to increase the nonlinearity so as to overcome the decoherence. In our proposed composite system the nonlinear coefficient χ can be large enough so that the squeezing and the NOON state can be obtained in a short time, which is very important in view of decoherence. Moreover, the additional dissipation induced by the MNP has little effect on the system because here the dipole emitters interact dispersively with the cavity modes.

In summary, we have studied a composite MNP-WGM coupling system. With the help of the MNP, the single-photon coupling strength between a dipole emitter and the cavity system can be substantially enhanced, while the high-Q property is preserved. The single-atom cooperativity obtains a more than two orders of magnitude increase compared with the conventional WGM cavity QED system. Also, the MNP-induced coupling enhancement covers a broad band up to several hundred nanometers so that the microcavity and the MNP do not have to be on resonance. The system is applicable ranging from quantum optics to quantum information science. It also offers opportunities to exploit both theoretical and experimental physics in a stronger light-matter interaction regime, such as nonlinear optics (e.g., enhanced Raman and Rayleigh scattering) and highly sensitive biosensing (e.g., single nanoparticle sizing with an improved detection limit).

Y.F.X. thanks Edo Waks for stimulating discussions. This work was supported by NSFC (No. 11004003, No. 11023003, and No. 11121091), 973 program (No. 2007CB307001), and RFDPH (No. 20090001120004).

[1] H. Mabuchi and A. C. Doherty, Science **298**, 1372 (2002).
[2] R. Miller *et al.*, J. Phys. B **38**, S551 (2005).
[3] S.-B. Zheng and G.-C. Guo, Phys. Rev. Lett. **85**, 2392 (2000).
[4] T. Pellizzari, S. A. Gardiner, J. I. Cirac, and P. Zoller, Phys. Rev. Lett. **75**, 3788 (1995); L.-M. Duan and H. J. Kimble, *ibid.* **92**, 127902 (2004).
[5] J. I. Cirac, P. Zoller, H. J. Kimble, and H. Mabuchi, Phys. Rev. Lett. **78**, 3221 (1997); W. Yao, R.-B. Liu, and L. J. Sham, *ibid.* **95**, 030504 (2005).
[6] G. Khitrova *et al.*, Nat. Phys. **2**, 81 (2006).
[7] D. J. Alton *et al.*, Nat. Phys. **7**, 159 (2011); S. Schietinger, T. Schroder, and O. Benson, Nano Lett. **8**, 3911 (2008); K. Srinivasan and O. Painter, Nature (London) **450**, 862 (2007); N. Le Thomas *et al.*, Nano Lett. **6**, 557 (2006); Y.-S. Park *et al.*, *ibid.* **6**, 2075 (2006); T. Aoki *et al.*, Nature (London) **443**, 671 (2006); E. Peter *et al.*, Phys. Rev. Lett. **95**, 067401 (2005).
[8] E. Hutter and J. H. Fendler, Adv. Mater. **16**, 1685 (2004).
[9] M. Pelton, J. Aizpurua, and G. Bryant, Laser Photon. Rev. **2**, 136 (2008).
[10] W. Zhang, A. O. Govorov, and G. W. Bryant, Phys. Rev. Lett. **97**, 146804 (2006).
[11] R. D. Artuso and G. W. Bryant, Nano Lett. **8**, 2106 (2008).
[12] A. Ridolfo, O. Di Stefano, N. Fina, R. Saija, and S. Savasta, Phys. Rev. Lett. **105**, 263601 (2010).
[13] S. Savasta *et al.*, ACS Nano **4**, 6369 (2010).
[14] E. Waks and D. Sridharan, Phys. Rev. A **82**, 043845 (2010).
[15] D. F. Walls and G. J. Milburn, *Quantum Optics*, 2nd ed. (Springer, Berlin, 2008).
[16] B. Min *et al.*, Nature (London) **457**, 455 (2009).
[17] Y.-F. Xiao *et al.*, Phys. Rev. Lett. **105**, 153902 (2010).
[18] D. K. Armani, T. J. Kippenberg, S. M. Spillane, and K. J. Vahala, Nature (London) **421**, 925 (2003).
[19] D. Ratchford, F. Shafiei, S. Kim, S. K. Gray, and X. Li, Nano Lett. **11**, 1049 (2011).
[20] J. Merlein *et al.*, Nat. Photon. **2**, 230 (2008).
[21] A. Mazzei *et al.*, Phys. Rev. Lett. **99**, 173603 (2007); J. Zhu *et al.*, Nat. Photonics **4**, 46 (2010).
[22] K. L. Kelly, E. Coronado, L. L. Zhao, and G. C. Schatz, J. Phys. Chem. B **107**, 668 (2003).
[23] M. Barth *et al.*, Nano Lett. **10**, 891 (2010).
[24] P. B. Johnson and R. W. Christy, Phys. Rev. B **6**, 4370 (1972).
[25] M. L. Andersen, S. Stobbe, A. S. Sörensen, and P. Lodahl, Nat. Phys. **7**, 215 (2011).
[26] E. Dulkeith *et al.*, Nano Lett. **5**, 585 (2005).

[27] P. Anger, P. Bharadwaj, and L. Novotny, Phys. Rev. Lett. **96**, 113002 (2006).

[28] L. Rogobete, F. Kaminski, M. Agio, and V. Sandoghdar, Opt. Lett. **32**, 1623 (2007); H. Mertens and A. Polman, J. Appl. Phys. **105**, 044302 (2009).

[29] C. W. Gardiner and P. Zoller, *Quantum Noise*, 3rd ed. (Springer, Berlin, 2004).

[30] Y.-C. Liu *et al*., Phys. Rev. A **84**, 011805(R) (2011).

[31] M. J. Kastoryano, F. Reiter, and A. S. Sørensen, Phys. Rev. Lett. **106**, 090502 (2011); Y.-F. Xiao, X.-B. Zou, and G.-C. Guo, Phys. Rev. A **75**, 012310 (2007).

[32] M. Kitagawa and M. Ueda, Phys. Rev. A **47**, 5138 (1993).

[33] I. Afek, O. Ambar, and Y. Silberberg, Science **328**, 879 (2010).

[34] G. R. Jin *et al*., New J. Phys. **11**, 073049 (2009).